



Super-Lift and Thrusting Airfoil of Coflow Jet Actuated by Micro-Compressors

Gecheng Zha, * Yunchao Yang, † Yan Ren, ‡ Brendan McBreen §
Dept. of Mechanical and Aerospace Engineering
University of Miami, Coral Gables, Florida 33124
E-mail: gzha@miami.edu

Abstract

This paper presents the wind tunnel experimental study of coflow jet (CFJ) active flow control airfoils actuated by micro-compressors embedded inside the airfoils. This is the first time that a CFJ airfoil is successfully controlled by the self-contained zero-net mass-flux (ZNMF) system. It is a crucial step to bringing the CFJ airfoil to practical aerospace applications. Furthermore, this study proves for the first time in experiment that a CFJ airfoil can achieve a Super-Lift Coefficient (SLC), which exceeds the theoretical limit of potential flow theory defined by $C_{Lmax} = 2\pi(1 + t/c)$. The CFJ airfoils studied in this research were modified from the NACA 6421 airfoil geometry with a size of 0.72 m \times 2.1 m (chord \times span). Two airfoils were tested, one with larger injection slot size for high cruise efficiency and low CFJ power consumption, the other with smaller injection size to achieve high C_{Lmax} for takeoff/landing. The freestream velocity varies from about 4.8m/s to 16.2m/s while the Reynolds number varies from 208,000 to 691,000. The C_{Lmax} of 8.6 is achieved by the high lift takeoff/landing configuration at the low freestream speed of 4.8m/s. The CFJ airfoil also generates very high thrust with the thrust coefficient up to about 1.0. The thrust is maintained up to the airfoil stall at 40° AoA with a drag of $C_D = -0.5$. Since the micro-compressors and the CFJ airfoil were designed separately, they do not work optimally together in the experiment. The micro-compressor operating line is substantially lower than the designed operating line with a severe penalty to the compressor efficiency. Future micro-compressor design needs to be tightly incorporated with the CFJ airfoil operating conditions to make use of the high compressor efficiency.

Nomenclature

<i>EBF</i>	External Blown Flaps
<i>IBF</i>	Internal Blown Flap
<i>CESTOL</i>	Cruise-Efficient Short Takeoff and Landing
<i>ESTOL</i>	Extreme Short Take-Off and Landing
<i>AoA</i>	Angle of Attack
<i>AFC</i>	Active Flow Control
<i>CFJ</i>	Co-Flow Jet
<i>FASIP</i>	Flow-Acoustics-Structure Interaction Package

* Professor, ASME Fellow, AIAA associate Fellow

† Ph.D. Candidate, AIAA student member

‡ Postdoc, AIAA member

§ Ph.D. Student

Approved for public release; distribution is unlimited.

<i>LE</i>	Leading Edge
<i>TE</i>	Trailing Edge
<i>RANS</i>	Reynolds-Averaged Navier-Stokes
<i>ZNMF</i>	Zero-Net Mass Flux
<i>P</i>	CFJ pumping power, $P = \frac{\dot{m}C_p T_{t2}}{\eta} (\Gamma^{\frac{\gamma-1}{\gamma}} - 1)$
η	CFJ pumping system efficiency, propeller efficiency
P_c	Power coefficient, $P_c = \frac{P}{\frac{1}{2}\rho_\infty V_\infty^3 S}$
<i>PR</i>	Total pressure ratio, Γ
C_L	Lift coefficient
C_D	Drag coefficient
C_M	Moment coefficient
C_μ	Jet momentum coefficient, $C_\mu = \frac{\dot{m}V_j}{\frac{1}{2}\rho_\infty V_\infty^2 S}$
C_{Lmax}	Maximum lift coefficient
$(L/D)_c$	Aerodynamic efficiency corrected for CFJ airfoil, $\frac{L}{D+P/V_\infty}$
C_{RW}	Aircraft Productivity parameter
C_L^2/C_D	Productivity efficiency coefficient
$(C_L^2/C_D)_c$	Productivity efficiency coefficient corrected for CFJ airfoil, $(C_L^2/C_D)_c = C_L^2/(C_D + P_c)$
R	Aircraft range
\bar{W}	Aircraft averaged weight during cruise
Re	Reynolds number
M	Mach number
M_{is}	Isentropic Mach number
C_p	Pressure coefficient
c_p	Constant pressure specific heat
γ	Air specific heats ratio
S	Planform area of the wing
ρ_∞	Freestream density
V_∞	Freestream velocity
T_t	Total temperature
P_t	Total pressure
H_t	Total enthalpy
α	Angle of attack
\dot{m}	Mass flow
C	Chord length
j	Subscript, stands for jet
c	Subscript, stands for corrected

1 Introduction

An airfoil, typically shaped as a round blunt leading edge and a sharp trailing edge, is the fundamental element of man made fluid machinery such as aircraft, wind turbines, turbomachinery, propellers, etc. For example, an aircraft wing or wind turbine blade is usually formed by stacking a series of airfoils along a span. A conventional airfoil’s major function is to generate lift. It also unavoidably comes with drag generated from surface friction and pressure distribution. For a man made system, the drag is typically overcome by a separate system such as the engines on an airplane. In nature, birds obtain both lift and thrust from their flapping wings, attributed to the very low pressure of the super-suction effect at leading edge at powered downstroke. Because of its profound impact on industrial applications, study of airfoil high lifting and thrusting behavior is an important subject of aerodynamics.

Maximum lift coefficient, C_{Lmax} , is very important to determine an airplane’s takeoff/landing distance and noise level. The higher the C_{Lmax} , the shorter the takeoff/landing distance, and the lower the airframe noise due to smaller stall velocity. Achieving high C_{Lmax} is hence critical to increase future airport capacity and reduce airport community noise.

Smith[1] pioneered the research of high lift fluid mechanics and gave a C_{Lmax} limit below based on potential flow:

$$C_{Lmax} = 2\pi(1 + \frac{t}{c}) \quad (1)$$

A necessary condition to achieve this solution is that the airfoil must satisfy the Kutta condition at the sharp trailing edge, which allows the potential flow to have a unique solution. The Kutta condition also enforces the trailing edge as a stagnation point location. The potential flow theory achieves the C_{Lmax} limit at the angle of attack (AoA) of 90° since a potential flow will not be stalled. For the CFJ-NACA-6421 airfoil studied in this paper, the theoretical C_{Lmax} is 7.6.

If a cylinder potential flow is forced to satisfy the Kutta condition (e.g. by adding a tiny sharp tail at the bottom), Eq. (1) also applies and it gives the C_{Lmax} of 4π [1] with the stagnation point located at the very bottom of the cylinder. In Prandtl’s pioneering rotating cylinder experiment, Prandtl considered 4π as the C_L limit[2]. For a cylinder potential flow with no sharp trailing edge, the Kutta condition is not a necessary condition and the lift coefficient can be greater than 4π with the stagnation point detached from the cylinder surface. The lift coefficient exceeding 4π was proved in 1993 by Tokumaru and Dimotakis [3] in their rotating cylinder experiment, which obtained a lift coefficient of nearly 16. In principle, there is no lift coefficient limit for a cylinder if the circulation added to the flow can be continuously increased. However, in Tokumaru and Dimotakis’s experiment [3], the lift coefficient tends to be plateaued when the rotating cylinder angular velocity continues to be increased. This is because when the angular velocity is too large, the viscosity at a very high Reynolds number is not sufficient to transfer the vorticity and the flow on the cylinder surface becomes “slippery”. In that case, the flow is not able to continue absorbing the mechanical energy from the rotating cylinder to increase circulation.

A cylinder is a good lift generating device with a high lift coefficient, but it comes with large pressure drag due to the blunt shape with no sharp trailing edge. It is hence rarely used as a complete lifting device that requires the drag to be minimal. For slender airfoils with sharp trailing edges, the C_{Lmax} limit of Smith’s theory [1] had been perceived as unsurpassable. Smith demonstrated that a 7-element flap system could achieve a C_{Lmax} close to 4. Zha and his team [4, 5, 6, 7] have achieved a C_{Lmax} of about 5 using CFJ flow control. These C_{Lmax} values are still far from the limit and until recently, Smith’s lift coefficient limit[1] has remained unchallenged.

In 2017, Yang and Zha [8] numerically obtained airfoil lift coefficients exceeding the theoretical limit using CFJ active flow control based on Reynolds Averaged Navier-Stokes (RANS) equations. A lift coefficient greater than

the theoretical limit is termed a Super-Lift Coefficient (SLC) [8].

The CFJ airfoil is an airfoil active flow control concept recently developed by Zha and his team [4, 5, 6, 7, 8, 9, 10, 11, 12, 13, 14]. As sketched in Fig. 1, a CFJ airfoil draws a small amount of mass flow into the airfoil near the trailing edge, pressurizes and energizes it using a micro-compressor actuator embedded inside the airfoil, then tangentially injects the same mass flow near the leading edge in the main flow direction. The CFJ airfoil does not add any mass flow to the airfoil system and thus is a zero-net-mass-flux (ZNMF) system.

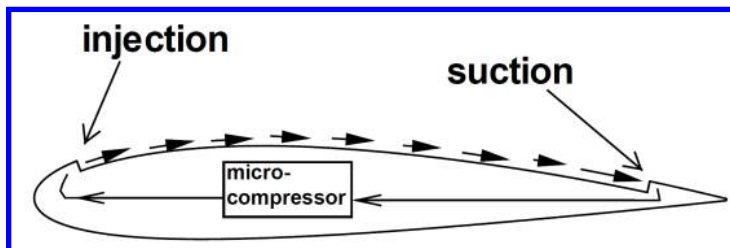


Figure 1: Sketch of a CFJ Airfoil.

The fundamental mechanism of the CFJ airfoil is that the turbulent mixing via large vortex structures between the jet and main flow energizes the wall boundary-layer, which allows the flow to overcome an extremely severe adverse pressure gradient and remain attached at a very large angle of attack with an extraordinarily high lift coefficient [15]. The CFJ airfoil has very low energy expenditure, because the jet is injected at the leading edge peak suction location, where the main flow pressure is near the lowest and it hence requires a low power to eject the flow, and it is sucked at the trailing edge, where the main flow pressure is near the highest and it hence requires a low power for the flow to be sucked into the airfoil. The low energy expenditure is the key factor enabling the CFJ airfoil not just to achieve ultra-high lift coefficient at high AoA, but also to possess a unique capability to improve aerodynamic efficiency at cruise when the flow is benign at low AoA from subsonic to transonic [7, 13, 14].

The CFD simulation of Yang and Zha [8] indicates that when a SLC occurs, the circulation is so high that the stagnation point is detached from the airfoil body similar to a cylinder flow as shown in Fig. 2, which has a C_{Lmax} of 10.6, far greater than the theoretical limit of 7.6. The freestream condition has a Mach number of 0.063 and Reynolds number of 3 million. The flow remains attached at AoA of 70° and the wake is filled with reversed velocity deficit, similar to the owl effect. For Reynolds number greater than 100,000, our past numerical simulation and wind tunnel testing indicate that the CFJ airfoil performance is not sensitive to variations of Reynolds number. This is because that the CFJ injection near leading edge always triggers the boundary layer transit to turbulence. The CFJ airfoil pressure coefficient at the leading edge suction peak is nearly 10 times higher than the maximum value of the baseline airfoil at AoA of 18° before it stalls [8]. In other words, the CFJ airfoil at SLC condition can keep flow attached despite an adverse pressure gradient nearly one order of magnitude higher than the conventional airfoil.

The Kutta condition is not satisfied for the flow around the CFJ airfoil trailing edge when the SLC occurs, as shown in Fig. 2. The potential flow C_{Lmax} of an airfoil is a result of enforcing the Kutta condition[1], which is a purely mathematical condition that includes only a subset of flow field solutions. Therefore, breaking the Kutta condition does not necessarily violate the laws of physics governed by the Navier-Stokes Equation, rather, it expands our understanding of fluid mechanics into new territory.

The simulation of Yang and Zha [8] also reveals a complex phenomenon with 4 layers of counter-rotating vortex layers emanating from leading edge and trailing to the wake of the airfoil as shown in Fig. 3. The wall boundary layer generates the first layer clock-wise vortex sheet on the airfoil surface. A turbulent mixing shear layer is formed starting from the lip of the injection duct between the high momentum injection jet and the boundary

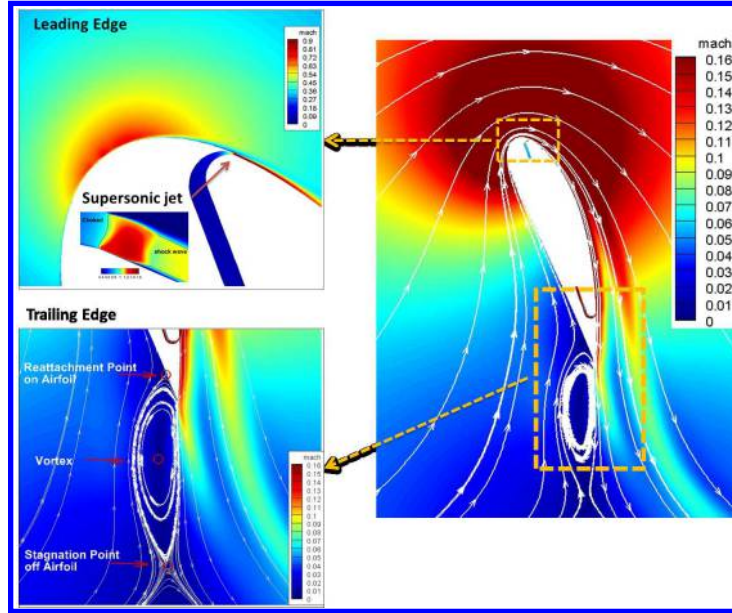


Figure 2: Mach number contours and streamlines at $C_{\mu} = 0.35$ and $\text{AoA} = 70^{\circ}$ for the CFJ6421-SST016-SUC053-INJ009 airfoil.

layer from the upstream of the very leading edge. Between the wall surface clock-wise boundary layer vortex layer and the shear layer, a counter-clockwise CFJ vortex layer is generated downstream of the CFJ injection slot due to the high speed of the coflow jet. Outside of the injection jet mixing layer is a clockwise vortex layer, which is induced by the CFJ via the mixing layer, namely induced vortex layer. The induced vortex layer further induces a jet turning around the leading edge, namely secondary induced jet, as shown in green color in Fig. 3. The secondary induced jet creates a counter clockwise vortex layer, namely transitional vortex layer, to transit the velocity to the slower freestream velocity.

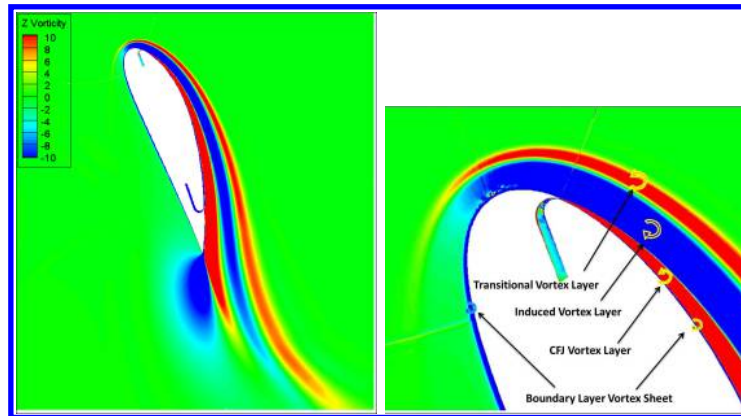


Figure 3: Vorticity contour at $C_{\mu} = 0.35$ and $\text{AoA} = 70^{\circ}$ for the CFJ6421-SST016-SUC053-INJ009 airfoil.

Among the 4 vortex layers, the clockwise vortices contribute to lift generation with the enhanced circulation. The counter clockwise vortices contribute to thrust generation with reversed wake velocity deficit. The CFJ is the source inducing the multiple vortex layers, which provide the energy to resist the extremely high adverse pressure gradient and keep the flow attached at very high AoA.

Yang and Zha [8] conclude based on their CFD simulation that there is no theoretical limit of airfoil lift coefficient. The actual lift coefficient limit of an airfoil depends how much energy the airfoil flow can absorb from external energy source to overcome the extremely severe adverse pressure gradient and keep the flow attached. In other words, the lift coefficient depends on how much and how effective an active flow control can transfer external energy to the airfoil flow.

The vortex structures and their directions of the SLC CFJ airfoil may be explained by the steady state Navier-Stokes equations due to energy transfer in the form of[15]:

$$\mathbf{V} \times \boldsymbol{\Omega} = \nabla H_t - T \nabla S - F_{viscous} \quad (2)$$

where \mathbf{V} is the flow velocity vector, $\boldsymbol{\Omega}$ is the vorticity vector, H_t is the total enthalpy, S is the entropy, and $F_{viscous}$ is the viscous force. However, the detailed analysis of the qualitative flow mechanism is not the focus of this paper. A more important question before studying the detailed flow mechanism is whether or not such an ultra-high adverse pressure gradient flow for an airfoil is quantitatively achievable in physics. If not, the SLC will remain a hypothetical based on steady state RANS simulation.

The purpose of this study is to conduct wind tunnel experiments and prove quantitatively the existence of the airfoil super-lift coefficient with ultra-high thrust. This is the necessary first step to explore this new area of fluid mechanics.

2 The CFJ Airfoils

The CFJ airfoils studied in this research were modified from the NACA 6421 airfoil geometry with a size of 0.72 m × 2.1 m (chord × span). Two CFJ airfoil configurations are tested in this study, one for takeoff/landing to maximize the lift coefficient, one for cruise to maximize the aerodynamic and productivity efficiency. Both airfoils are numerically studied by Yang and Zha in[8]. The CFJ airfoil is modified from the NACA 6421 airfoil by making a suction surface translation(SST) downward. Fig. 4 shows several CFJ airfoil geometries with various SST, injection slot sizes and suction slot sizes in the trade study conducted in [8].

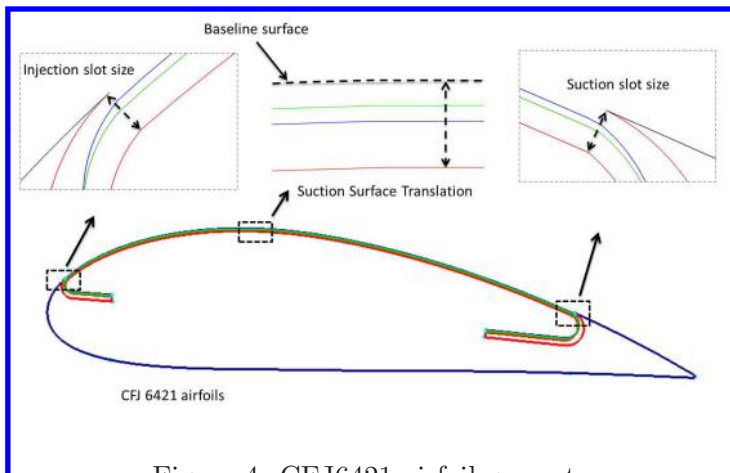


Figure 4. CFJ6421 airfoil geometry

In general, to have high C_{Lmax} , it is more effective to have smaller injection size with higher injection velocity, which will give higher injection jet momentum and lower mass flow rate if the C_μ is fixed. However, the power coefficient of the CFJ airfoil is also high with smaller injection size because the jet suffers high energy loss going

through small holes. At cruise a high efficiency is more important, so a larger injection slot size with lower jet velocity and thus lower loss is more desirable.

Table 1 gives the detailed parameters of the two CFJ airfoils designed for takeoff/landing and cruise condition, including the injection and suction slot size normalized by chord length(C), and the injection jet momentum coefficient used. The 3-digit number in the naming convention stands for the SST distance, injection slot size, and suction slot size normalized by the airfoil chord.

Table 1: CFJ6421 airfoil geometry parameters for takeoff/landing and cruise condition

Case	CFJ6421 airfoil	SST (%C)	SUC slot size (%C)	INJ slot size (%C)
Takeoff/Landing	SST016-SUC053-INJ009	0.16	0.53	0.09
Cruise	SST143-SUC133-INJ065	1.43	1.33	0.63

2.1 Subsonic Wind Tunnel

The Texas A&M Oran W. Nicks Low Speed Wind Tunnel (LSWT) is used for the wind tunnel testing of this research. The LSWT is a large-scale, closed-circuit wind tunnel located at Easterwood Airport in College Station, Texas. A schematic of the facility is given in Fig. 11.

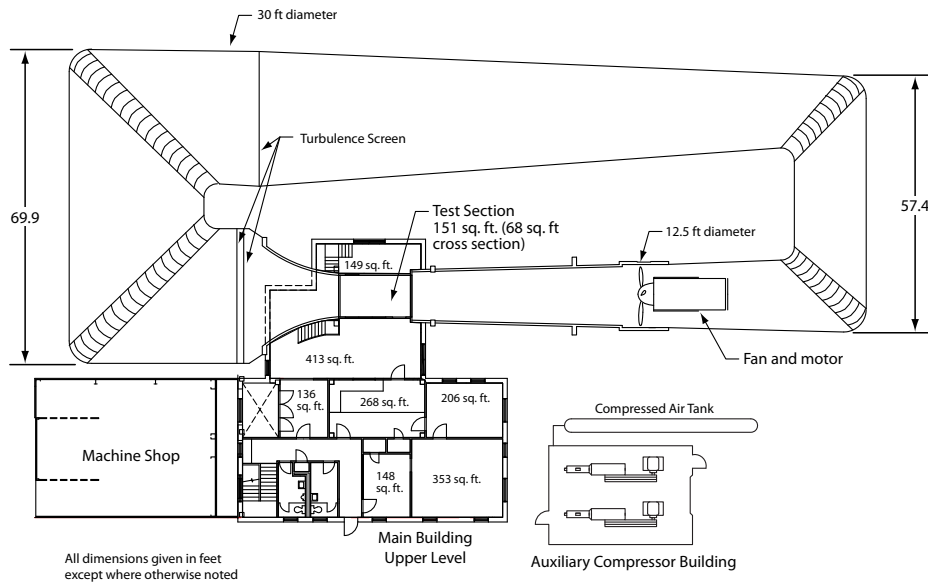


Figure 5: Schematic view of the LSWT at TAMU.

The rectangular test section is 7 feet tall, 10 feet wide, and 12 feet in length. The test section contains one-foot chamfers in all four corners that reduce the overall cross sectional area to 68 square feet. The walls diverge two inches in the horizontal direction over the length of the test section to account for boundary layer growth and minimize stream-wise buoyancy. Two vertical vent slots allow the tunnel to maintain a static pressure in the test section near ambient. A 46-foot-long diffuser, located downstream of the test section, changes the cross sectional shape from rectangular, back to circular at the fan.

The test section can be outfitted with a three axis traversing mechanism. The tunnel is controlled using the calculated dynamic pressure of the airflow at the center of the test section. Two static pressure rings, consisting of four ports each, are used to measure the average static pressure in the tunnel at the end of the settling chamber and five feet in front of the test section. The difference of these static pressure measurements is a pseudo dynamic pressure called q_{set} . The measurement of q_{set} is used to calibrate the actual dynamic pressure in the center of the empty test section, q_{act} , with the use of a Pitot tube. A calibration curve is created and used to calculate q_{act} from set when the Pitot tube is not installed in the test section. While the tunnel is in operation, q_{set} is constantly measured and used to calculate q_{act} .

The temperature inside the tunnel is measured with a thermocouple that is located on the wall at the beginning of the test section. The barometric pressure is recorded in the balance room, beneath the test section. These measurements allow the velocity in the test section, based on tunnel conditions, to be calculated in real-time. The total and static pressure in the tunnel are also measured during a test, with use with a Pitot tube located on the far wall.

LSWT is equipped with a six component, pyramidal electromechanical, external balance system located beneath the test section. The external balance measures three force components and three moments in a wind-oriented coordinate system. The origin of the coordinate system is the geometric center of the test section, 42 inches above the floor. The measurements are sent to the data acquisition system using optical encoders. Lift force can be measured from -1000 lbf to +3000 lbf, while drag and side force can be measured from ± 1000 lbf. Pitching and rolling moments can be measured to ± 2000 ft-lbf, while yaw can be measured to ± 1000 ft-lbf. Force and moments are accurate to 0.1% of the applied load or moment, with a minimum accuracy of 0.1 lbf or ft-lbf, respectively. The external balance is isolated from the upper turntable. The turntable can rotate to any yaw angle (ψ) orientation within -120° to $+190^\circ$. LSWT can also be equipped with an internal balance system for other tests.

3 Results and Discussion

Table 2 is the wind tunnel testing conditions with the dynamic pressure varied from 0.3Q to 3Q. The Q has the dynamic pressure equal to 1psf. The velocity is varied from 4.84m/s to 16.26m/s and the Reynolds number is from 208588 to 691126. The CFJ airfoil has 5 micro-compressors embedded inside along the span as shown in 6.

Table 2: Wind Tunnel Testing Conditions

Case	Velocity(m/s)	Reynolds number
0.3Q	4.84	208,588
0.5Q	6.25	269,078
1Q	9.39	399,022
2Q	13.27	564,217
3Q	16.26	691,126

The mixed centrifugal and axial compressor design micro-compressor has a outer diameter of 84mm and length of 124mm. The mass flow rate ranges from about 10g/s to 80g/s with the pressure ratio varying from 1.03 to 1.4. The maximum power of the compressor is 2kW. The micro-compressor is customer designed based on our CFD design and simulation of the CFJ airfoil matching the wind tunnel conditions. The aerodynamic design of the micro-compressor was conducted by PCA Limited in England[16]. The mechanical design and manufacturing of the micro-compressors are done by Celeroton in Switzerland[17]. Manufacturing such a small and high power compressor is very challenging. Fig. 8 is the compressor characteristics map showing the performance of the range

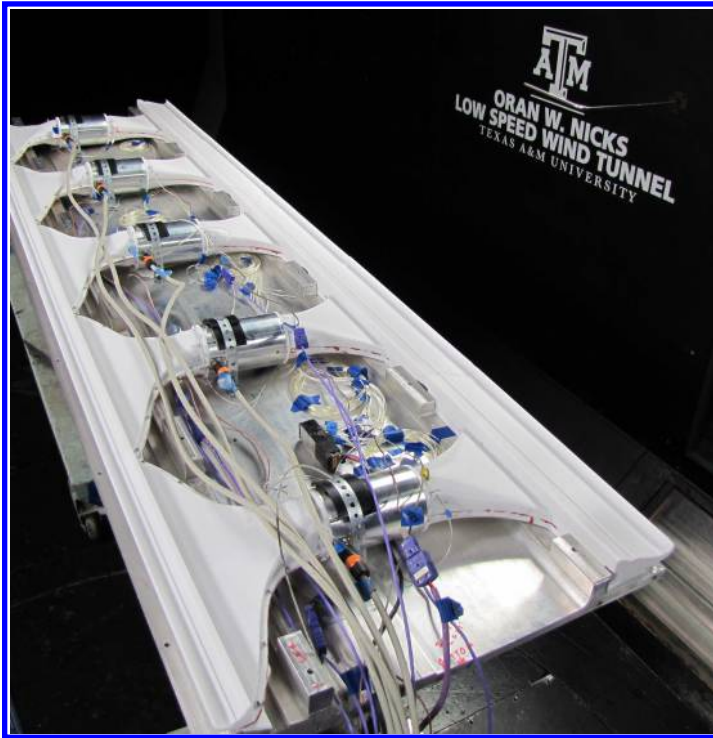


Figure 6: Photo of the tested CFJ-NACA-6421 airfoil with 5 micro-compressors embedded.

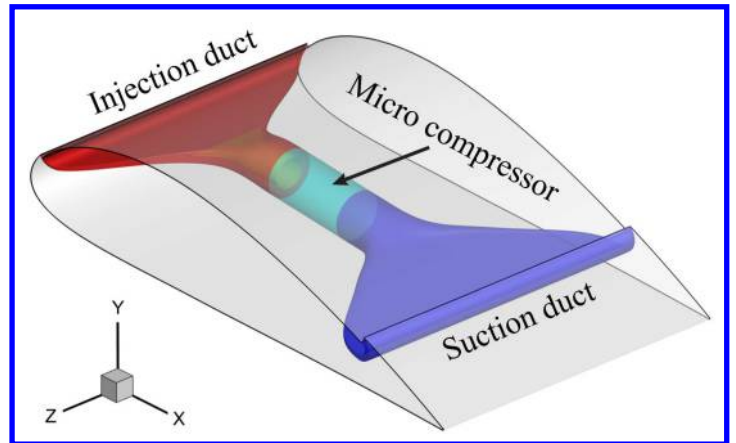


Figure 7: Sketch of the CFJ airfoil with the micro-compressor and the suction and injection duct.

of mass flow, pressure ratio and efficiency of the compressor at different corrected RPM ($n/\sqrt{T_0}$).

The CFJ airfoil takeoff/landing condition has smaller slot sizes than the cruise condition configuration. The injection slot size is largely varied. The micro-compressors hence experience the throttling effect similar to jet engines. Since CFJ airfoil generates very high thrust, the CFJ wing with embedded micro-compressors is a tightly integrated distributed propulsion system. The power consumed by CFJ enhances the lift and generates thrust simultaneously. This is different from a conventional propulsion system with the sole function to generate thrust.

Each compressor unit covers a span length of 0.42m as shown in Fig. 9. The ratio of the span width to the compressor inner diameter is 6.46. The duct has a shape of rectangle at the CFJ airfoil injection and suction slots, and then transits to a circular shape to match the compressor inlet and outlet interface. This brings a lot of challenges to design the injection and suction ducts with no flow separation. There are separated papers to report the duct simulation and design work[18, 19].

To save airfoil manufacturing cost, the two CFJ airfoil configurations for cruise and takeoff/landing share many common parts. Between the two configurations, the upper surface of the airfoil is translated by different amount to match the injection and suction slot size optimized by CFD. To match the injection duct contours, two leading edge parts are designed and manufactured respectively for the cruise and takeoff airfoils. There are a lot of detailed mechanical design and manufacturing to integrate the micro-compressors with the CFJ airfoil.

At the wind tunnel testing, each micro-compressor has a total pressure and static pressure probes at the compressor inlet and outlet. Three of the five compressors also have the temperature sensors at the inlet and outlet. The intent is to help to determine the mass flow rate and pressure ratio of the compressor. However, since the flow has high swirl at the outlet, the total pressure measurement has large uncertainty and is not very useful. The static pressure measurement is then used to have some approximate idea of the pressure ratio. Accurate

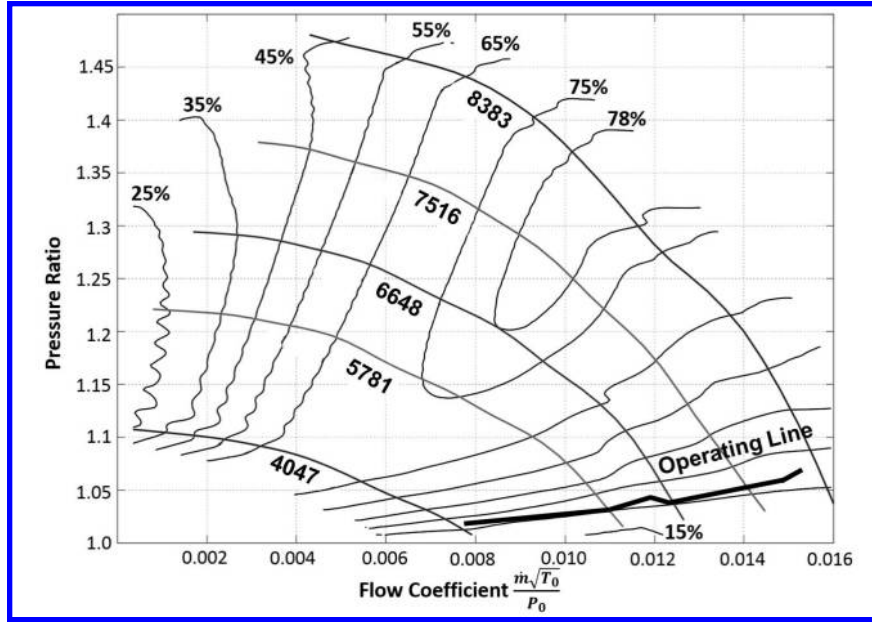


Figure 8: The characteristic map of the micro-compressor used as actuators for the CFJ airfoil.

measurement of the pressure ratio requires multiple pressure probes distributed circumferentially. So is for the temperature measurement. In the wind tunnel testing, the micro-compressors are controlled by different RPM to obtain different mass flow rate and pressure ratio. But accurate measurement of moment coefficient C_μ is not available. This will be left as future work.

Fig. 9 is the CFJ airfoil vertically mounted in the wind tunnel. The injection and suction slots are visible. Fig. 10 is the baseline airfoil tested for comparison. Since the injection slot is very small with the size less than 0.1% of the chord, the baseline airfoil is restored by simply sealing the injection slot with an aluminum tape. The suction slot has a larger size. A contoured wedge is 3D printed, inserted to the suction slot, and is merged with the suction surface. To ensure smoothness, the wedge is also taped as shown in Fig. 10. The treatment of the baseline airfoil is to save cost. Thus the baseline airfoil does not represent the exact NACA 6421 airfoil, but is very close with small deviation. It is sufficient to be used as a reference as uncontrolled baseline airfoil.

Fig. 12 to 15 are the coefficient of lift, drag and pitching moment, and drag polar plots of the cruise CFJ airfoil at 1Q condition compared with the baseline airfoil. The RPM is varied from 75k to 145k. The baseline airfoil has the maximum lift coefficient of 1.3 with fairly prolonged stall angle of attack. At the lowest RPM of 75k, the CFJ airfoil reaches the C_{Lmax} of 2, a 54% increase. At the RPM of 145k, the C_{Lmax} is 3.8, a 292% increase. Fig. 13 indicates that the CFJ airfoil achieves thrust for all the RPM at low AoA. The maximum thrust coefficient is about 0.18. For the high RPM of 145k, the thrust is maintained up to AoA of 28°. Fig. 15 shows that the nose down pitching moment is greater than that of the baseline airfoil. However, with the increase AoA and lift, the nose down pitching moment is decreased and approaches that of the baseline airfoil.

Fig. 16 to 19 are the coefficient of lift, drag and pitching moment, and drag polar plots of the high lift configuration of the CFJ airfoil for takeoff/landing at 1Q freestream condition. The maximum lift coefficient is increased to 5, a 385% improvement over the baseline airfoil. The thrust coefficient is also increased to 0.32.

Fig. 20 to 23 are the coefficient of lift, drag and pitching moment, and drag polar plots of the high lift CFJ airfoil under the condition that the super-lift coefficient is achieved. The CFJ airfoil configuration is the same as



Figure 9: Photo of the CFJ-NACA-6421 airfoil tested.

Figure 10: Photo of the baseline NACA 6421 airfoil.

the one for takeoff/landing. The purpose of this test is to prove that the lift coefficient can indeed exceed the theoretical limit of 7.6 as predicted by CFD[8]. Since the micro-compressors do not deliver enough mass flow to achieve sufficient injection momentum coefficient at 1Q freestream condition due to the off-design operating point, the freestream condition is reduced to 0.5Q and 0.3Q, which correspond to the freestream velocity of 6.25m/s and 4.84m/s. In the morning when the tunnel air is cooler, the C_{Lmax} reaches 9 at AoA of 30deg and freestream of 0.3Q. In the afternoon when the tunnel is hot, the compressors deliver less mass flow and the repeated tests obtained the C_{Lmax} of 8.6. They are all substantially higher than the limit of 7.6. This is the first time that an airfoil achieves the lift coefficient exceeding the theoretical limit. It is almost certain that the C_{Lmax} can go even higher with micro-compressors designed to deliver higher mass flow at the operating conditions. The maximum thrust coefficient is very large up to 1.0 at low AoA as shown in Fig.21. The thrust is maintained up to AoA of

40° with a value of $C_D = -0.5$. The pitching moment behaves similarly to the previous cases with nose down moment increased.

The compressor operating line in the experiment is estimated based on the limited measurement and the compressor map delivered by the manufacturer Celeroton. Fig. 8 shows that the compressor operating line is substantially lower than an operating line going through the design point that has the peak efficiency of slightly over 80%. The reason is that the compressor’s design point does not match the CFJ airfoil operating conditions because they are designed separately. The compressor was designed with the given conditions of total pressure ratio of 1.2 and an efficiency of 82% at the design point with a required mass flow rate of 50 g/s. These conditions are estimated based on the CFD simulation of the CFJ airfoil. By examining the 3D CFD results after the wind tunnel testing, it is observed that the total pressure ratio of the compressors is substantially higher than the CFJ airfoil’s total pressure loss. More importantly, the exit static pressure of the micro-compressor is much lower than that at the design point. The compressor is directly connected to the airfoil leading edge injection slot located at the suction peak point by a duct with fairly uniform area. The airfoil leading edge suction peak low pressure drives the compressor toward the choked condition at each constant RPM line, which positions the operating line far below the optimum efficiency region for which the compressor is designed.

Each of the five micro-compressors are dynamically controlled by CelerotonPilot via a CC-230-3500 electrical power converter. One converter controls one micro-compressor. With a user defined RPM setpoint, the 230 VAC current from the power supply is turned into a 0-360 Volt Pulse-Amplitude Modulated (PAM) current to match the RPM.

Converting the fixed frequency grid AC current to a variable frequency motor current comes with its associated energy losses, and converting the electrical energy to mechanical energy comes with still more. We measured energy losses at many levels while controlling the micro-compressors. Below is depicted an estimation of energy losses between the power supply and the electrical converter, the converter and the DC brushless motor, the motor and the shaft, and the shaft and the fluid flow. Because the micro-compressors were operating far from the peak efficiency point, the majority of the energy losses were found in transferring the mechanical energy to the fluid.

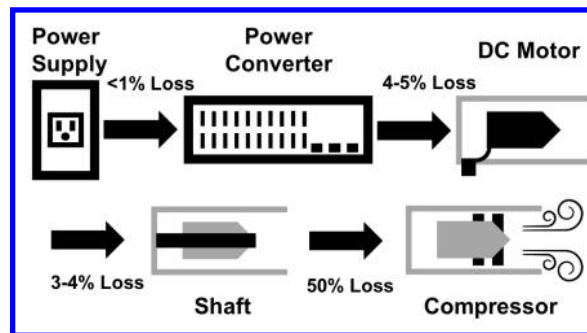


Figure 11: Estimation of energy losses between stages.

Table 3: System Efficiency Analysis, 115 kRPM

Converter Efficiency	94%
Motor Efficiency	95%
Compressor Efficiency	30%
System Efficiency	28%

Because this is the first experiment incorporating micro-compressors into the CFJ airfoil, it has been a learning

experience. Perhaps the most significant take away is that it is very necessary to closely couple CFJ airfoil design with the compressor design so that they both perform optimally at their operating conditions. This is similar to a jet engine with variable nozzle area to match the different flight conditions of an airplane's flight envelop.

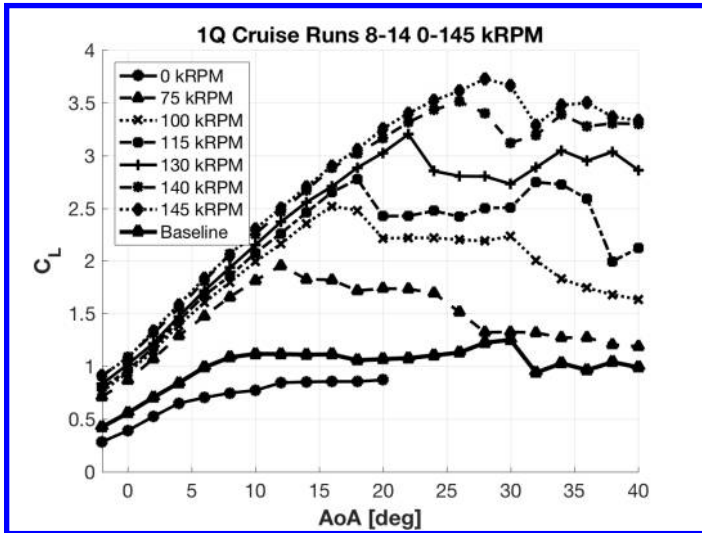


Figure 12: Cruise CFJ Lift Coefficient vs AoA.

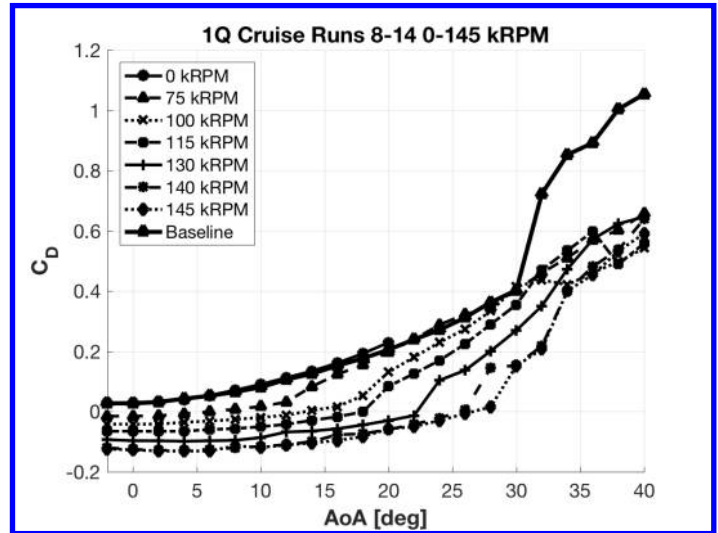


Figure 13: Cruise CFJ Drag coefficient vs AoA.

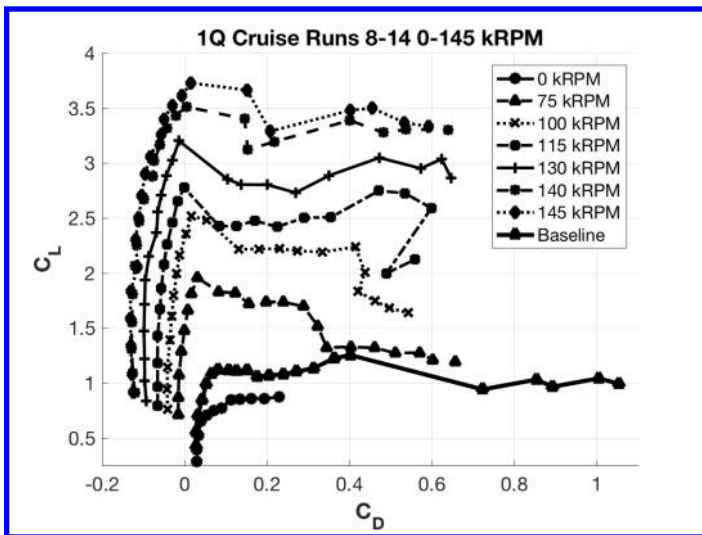


Figure 14: Cruise CFJ Drag Polar Plot.

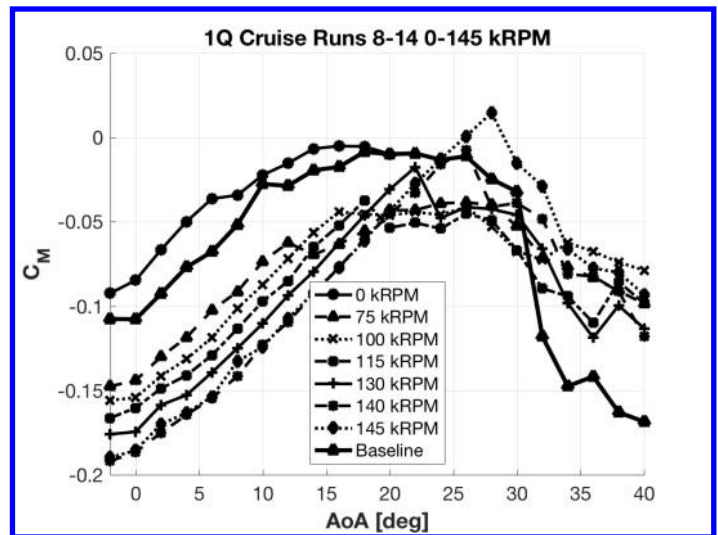


Figure 15: Cruise CFJ Moment coefficient vs AoA.

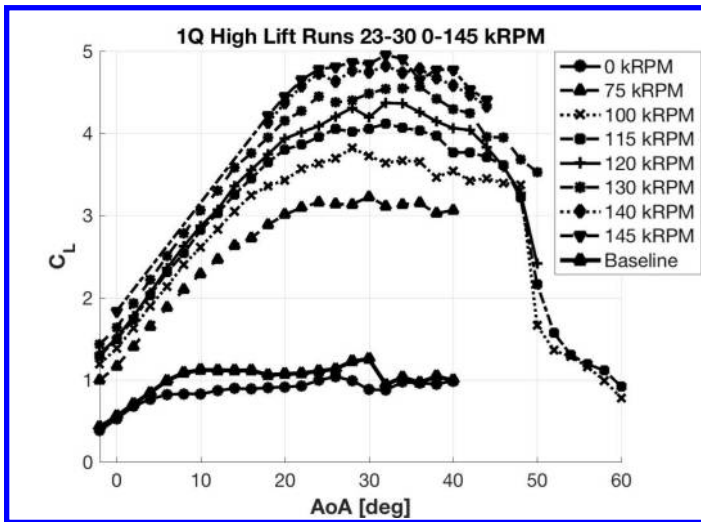


Figure 16: Takeoff/landing CFJ Lift Coefficient vs AoA.

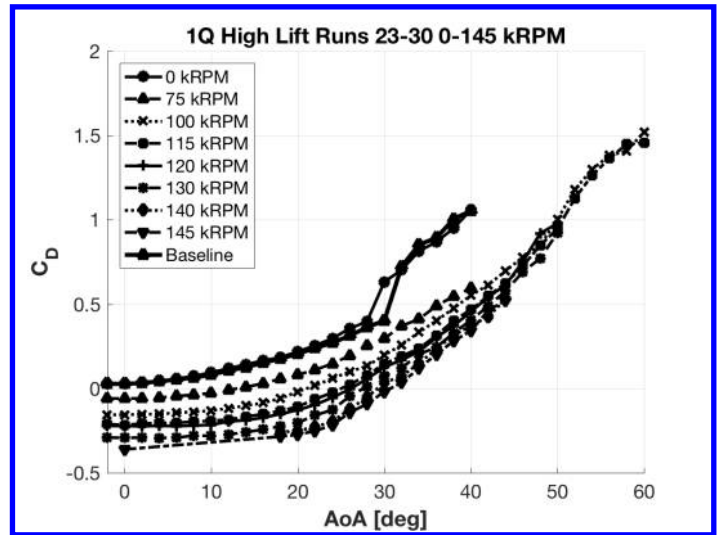


Figure 17: Takeoff/landing CFJ Drag coefficient vs AoA.

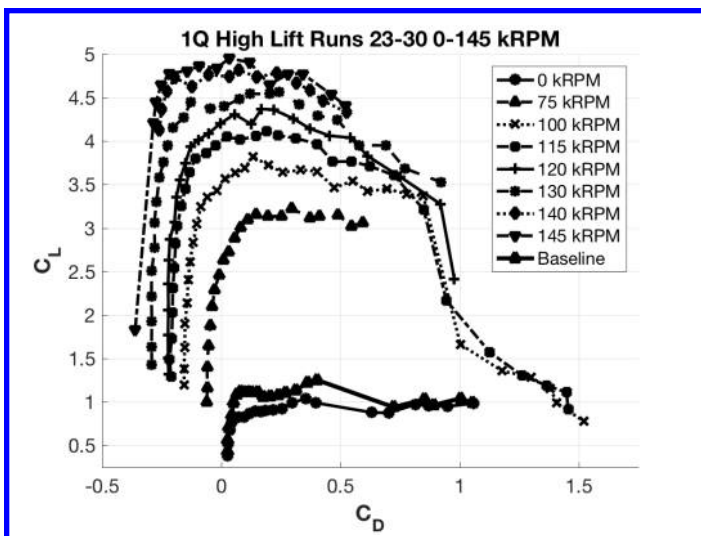


Figure 18: Takeoff/landing CFJ Drag Polar Plot.

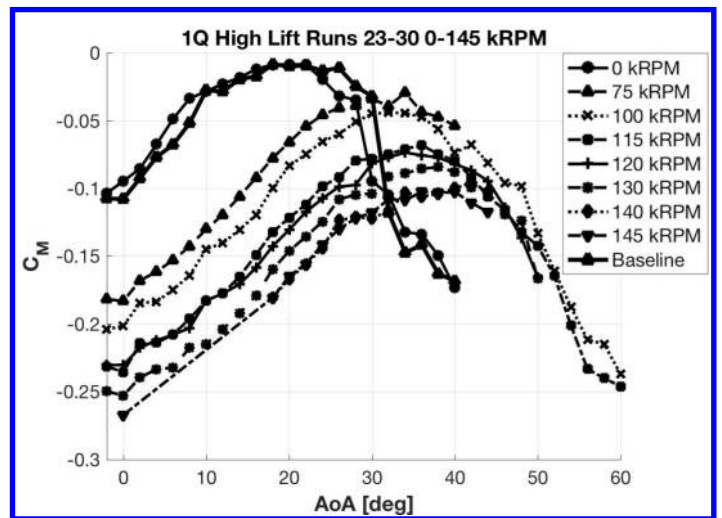


Figure 19: Takeoff/landing CFJ Moment coefficient vs AoA.

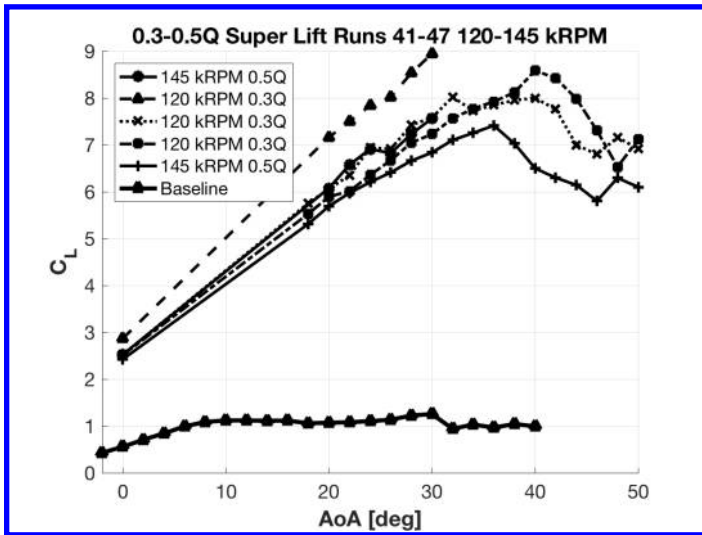


Figure 20: Super-Lift CFJ Lift Coefficient vs AoA.

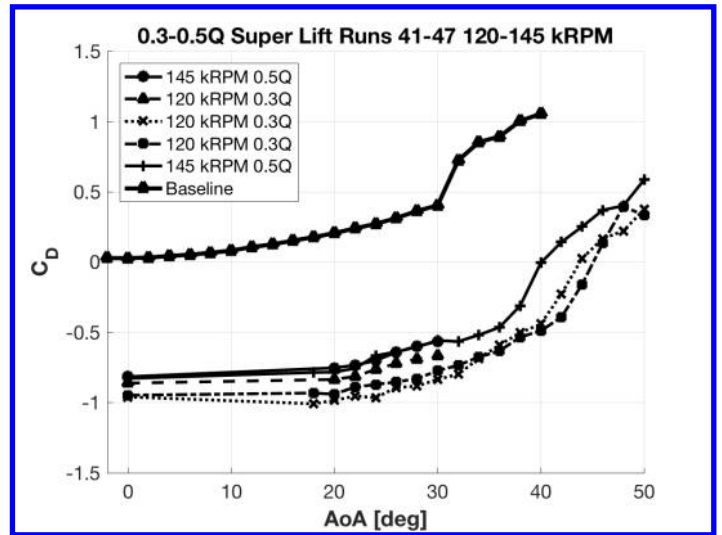


Figure 21: Super-Lift CFJ Drag coefficient vs AoA.

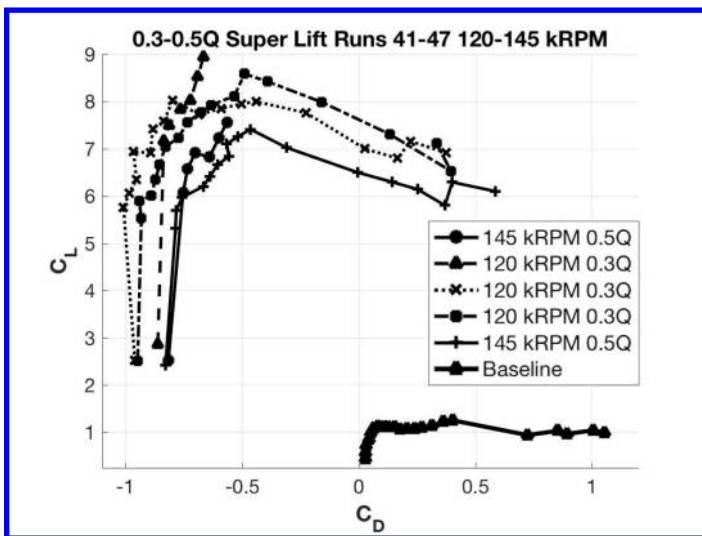


Figure 22: Super-Lift CFJ Drag Polar Plot.

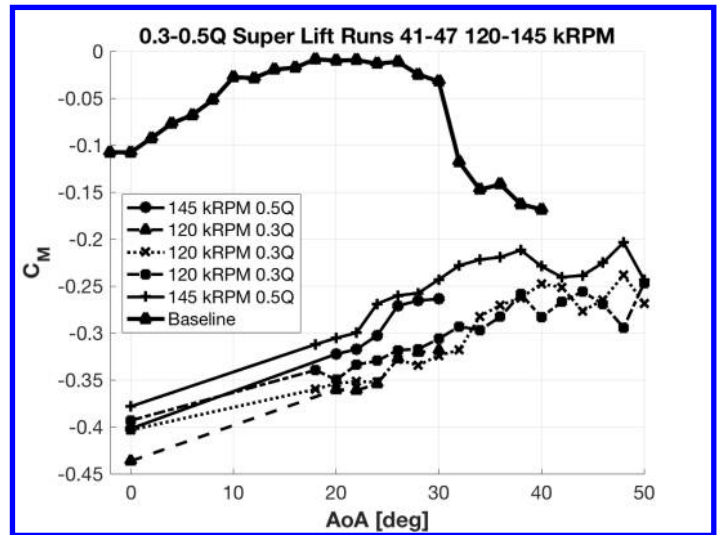


Figure 23: Super-Lift CFJ Moment coefficient vs AoA.

4 Conclusion

This paper successfully embeds micro-compressors into CFJ airfoil for the first time and demonstrate a radical lift coefficient enhancement, drag reduction, and increase of stall angle of attack by the self-contained ZNMF system. It is a crucial step to bring CFJ airfoil to practical aerospace applications. Furthermore, this study proves for the first time in experiment that a CFJ airfoil can achieve a Super-Lift coefficient(SLC), which exceeds the theoretical limit of potential flow theory defined by $C_{Lmax} = 2\pi(1 + t/c)$. The CFJ airfoil studied in this research was modified from NACA 6421 airfoil. Two sets of airfoil were tested, one with larger injection slot size to have high cruise efficiency and low CFJ power consumption, the other with smaller injection size to achieve high C_{Lmax} for takeoff/landing. The C_{Lmax} of 8.6 is achieved by the high lift takeoff/landing configuration at the low freestream speed of 4.8m/s. The CFJ airfoil also generates very high thrust with the thrust coefficient up to about 1.0. The thrust is maintained up to the airfoil is stalled at AoA of 40° with a value of $C_D = -0.5$. Since the micro-compressors and the CFJ airfoil are designed separately, they do not match well in the experiment. The micro-compressor operating line is substantially lower the the designed operating line with a severe penalty of the compressor efficiency. Future design of the micro-compressors needs to be tightly incorporated with the CFJ airfoil operating conditions to benefit the CFJ airfoil system from the high efficiency of the compressors.

5 Acknowledgment

This project is sponsored by the Defense Advanced Research Projects Agency and monitored by the program manager Jean-Charles Ledé under Cooperative Agreement No.: HR0011-16-2-0052. The content of the information does not necessarily reflect the position or the policy of the Government, and no official endorsement should be inferred. We thank Dr. Edward White and Ms. Lisa Brown and the team at the Teaxas A&M University Oran W. Nicks Low Speed Wind Tunnel facility for their help and support in conducting the wind tunnel testing. We also greatly appreciate the engineering services of PCA Engineers Ltd. for their aerodynamic design of the micro-compressor led by Dr. Chris Robinson, and Celeroton AG for their mechanical design, manufacturing, and testing of the micro-compressors, led by Mr. Christof Zwysig. The simulations are conducted on Pegasus supercomputing system at the Center for Computational Sciences at the University of Miami.

References

- [1] A. Smith, "High-Lift Aerodynamics," *Journal of Aircraft*, vol. 12, pp. 501–530, 1975.
- [2] T. O. G. Prandtl, Ludwig, *Applied Hydro- and Aeromechanics (Dover Books on Aeronautical Engineering)*. Dover Publications, 1934.
- [3] P. Tokumaru and P. Dimotakis, "The lift of a cylinder executing rotary motions in a uniform flow," *Journal of Fluid Mechanics*, vol. 255, pp. 1–10, 1993.
- [4] Zha, G.-C and Paxton, C. and Conley, A. and Wells, A. and Carroll, B., "Effect of Injection Slot Size on High Performance Co-Flow Jet Airfoil," *AIAA Journal of Aircraft*, vol. 43, 2006.
- [5] Zha, G.-C and Carroll, B. and Paxton, C. and Conley, A. and Wells, A., "High Performance Airfoil with Co-Flow Jet Flow Control," *AIAA Journal*, vol. 45, 2007.

- [6] B. P. E. Dano, G.-C. Zha, and M. Castillo, "Experimental Study of Co-Flow Jet Airfoil Performance Enhancement Using Micro Discreet Jets." AIAA Paper 2011-0941, 49th AIAA Aerospace Sciences Meeting, Orlando, FL,, 4-7 January 2011.
- [7] Lefebvre, A. and Dano, B. and Bartow, W. and Di Franzo, M. and Zha, G.-C., "Performance and Energy Expenditure of Co-Flow Jet Airfoil with Variation of Mach Number," *AIAA Journal of Aircraft*, vol. 53, pp. 1757–1767, 2016.
- [8] Yang, Y.-C. and Zha, G.-C., "Super-Lift Coefficient of Active Flow Control Airfoil: What Is the Limit?." AIAA Paper 2017-1693, AIAA SCITECH2017, 55th AIAA Aerospace Science Meeting, Grapevine, Texas, 9-13 January 2017.
- [9] Zha, G.-C. and Gao, W. and Paxton, C., "Jet Effects on Co-Flow Jet Airfoil Performance," *AIAA Journal*, No. 6,, vol. 45, pp. 1222–1231, 2007.
- [10] G.-C. Zha and D. C. Paxton, "A Novel Flow Control Method for Airfoil Performance Enhancement Using Co-Flow Jet." *Applications of Circulation Control Technologies*, Chapter 10, p. 293-314, Vol. 214, Progress in Astronautics and Aeronautics, AIAA Book Series, Editors: Joslin, R. D. and Jones, G.S., 2006.
- [11] Wang, B.-Y. and Haddoukessouni, B. and Levy, J. and Zha, G.-C., "Numerical Investigations of Injection Slot Size Effect on the Performance of Co-Flow Jet Airfoil ," *AIAA Journal of Aircraft*, vol. 45, pp. 2084–2091, 2008.
- [12] B. P. E. Dano, D. Kirk, and G.-C. Zha, "Experimental Investigation of Jet Mixing Mechanism of Co- Flow Jet Airfoil." AIAA-2010-4421, (5th AIAA Flow Control Conference, Chicago, IL), 28 Jun - 1 Jul 2010.
- [13] Lefebvre, A. and Zha, G.-C. , "Design of High Wing Loading Compact Electric Airplane Utilizing Co-Flow Jet Flow Control." AIAA Paper 2015-0772, AIAA SciTech2015: 53nd Aerospace Sciences Meeting, Kissimmee, FL, 5-9 Jan 2015.
- [14] Liu, Z.-X. and Zha, G.-C., "Transonic Airfoil Performance Enhancement Using Co-Flow Jet Active Flow Control." AIAA Paper 2016-3472, AIAA AVIATION 2016, 8th AIAA Flow Control Conference, Washington, D.C, June 13-17, 2016.
- [15] E. M. Greitzer, C. S. Tan, and M. B. Graf, "Internal Flows: Concepts and Applications." Cambridge University Press, Feb 26, 2007.
- [16] PCA engineers, "Design of a mixed flow fan." Internal Report to University of Miami, 2017.
- [17] Celeroton, "Design of a mixed flow fan prototype." Internal Report to University of Miami, 2017.
- [18] Y. Ren and G.-C. Zha, "Simulation of 3d co-flow jet airfoil with embedded micro-compressor actuator." AIAA Paper 2018-0330, AIAA SciTech Forum, 2018 AIAA Aerospace Sciences Meeting, Kissimmee, FL, 812 January 2018.
- [19] Y. Ren and G.-C. Zha, "Design of injection and suction ducts for coflow jet airfoils with embedded microcompressor actuator." AIAA Paper 2018-0330, AIAA SciTech Forum, 2018 AIAA Aerospace Sciences Meeting, Kissimmee, FL, 812 January 2018.